Research Article | Vol. 7, No. 8 | 1 Aug 2017 | OPTICAL MATERIALS EXPRESS 2880
Optical Materials EXPRESS

Gallium platinum alloys – a new material system for UV plasmonics

TING ZHANG,[1] YUNSHAN WANG,[2] KANAGASUNDAR APPUSAMY,[3] BING HUANG,[4] JINQI WANG,[2] FENG LIU,[4] STEVE BLAIR,[2] SIVARAMAN GURUSWAMY,[3] AND AJAY NAHATA[2,*]

[1]*Department of Physics and Astronomy, University of Utah, Salt Lake City, UT USA*
[2]*Department of Electrical and Computer Engineering, University of Utah, Salt Lake City, UT USA*
[3]*Department of Metallurgical Engineering, University of Utah, Salt Lake City, UT USA*
[4]*Department of Materials Science and Engineering, University of Utah, Salt Lake City, UT USA*
**nahata@ece.utah.edu*

Abstract: We describe a new material system based on alloys of gallium and platinum that is well-suited for ultraviolet (UV) plasmonics. Although gallium has previously been shown to be useful for such studies, creating a continuous, pinhole-free thin film has been technically challenging. For example, when vacuum deposition techniques are used, gallium forms as isolated spherical nanoparticles on a wide variety of substrates. We demonstrate that when a platinum wetting layer is deposited first on a substrate followed by a thick gallium layer, a Ga-Pt alloy thin film is formed near the interface. The excess surface gallium can then be removed using a focused ion beam (FIB), exposing the alloy film. Ellipsometry measurements show that the alloy largely retains the dielectric properties of solid gallium throughout the UV, although the properties of the two diverge somewhat in the visible. We fabricate periodic subwavelength aperture arrays in the alloy thin film and observe enhanced optical transmission resonances that are sharper in the UV than in the visible. The patterned films appear to be stable over time periods exceeding six months based on optical measurements.

OCIS codes: (160.3900) Metals; (250.5403) Plasmonics; (260.7190) Ultraviolet.

References and links (s

1. E. Ozbay, "Plasmonics: merging photonics and electronics at nanoscale dimensions," Science **311**(5758), 189–193 (2006).
2. M. Kauranen and A. V. Zayats, "Nonlinear plasmonics," Nat. Photonics **6**(11), 737–748 (2012).
3. A. G. Brolo, "Plasmonics for future biosensors," Nat. Photonics **6**(11), 709–713 (2012).
4. K. A. Willets, A. J. Wilson, V. Sundaresan, and P. B. Joshi, "Super-resolution imaging and plasmonics," Chem. Rev. **117**(11), 7538–7582 (2017), doi:10.1021/acs.chemrev.6b00547.
5. R. F. Chen, "Fluorescence quantum yields of tryptophan and tyrosine," Anal. Lett. **1**(1), 35–42 (1967).
6. C. R. Johnson, M. Ludwig, S. O'Donnell, and S. A. Asher, "UV resonance Raman spectroscopy of the aromatic amino acids and myoglobin," J. Am. Chem. Soc. **106**(17), 5008–5010 (1984).
7. G. D. Fasman, *Practical Handbook of Biochemistry and Molecular Biology* (CRC Press, 1989).
8. C. An, S. Peng, and Y. Sun, "Facile synthesis of sunlight-driven AgCl:Ag plasmonic nanophotocatalyst," Adv. Mater. **22**(23), 2570–2574 (2010).
9. S. K. Jha, Z. Ahmed, M. Agio, Y. Ekinci, and J. F. Löffler, "Deep-UV surface-enhanced resonance Raman scattering of adenine on aluminum nanoparticle arrays," J. Am. Chem. Soc. **134**(4), 1966–1969 (2012).
10. J. M. Sanz, D. Ortiz, R. Alcaraz de la Osa, J. M. Saiz, F. González, A. S. Brown, M. Losurdo, H. O. Everitt, and F. Moreno, "UV plasmonic behavior of various metal nanoparticles in the near- and far-field regimes: Geometry and substrate effects," J. Phys. Chem. C **117**(38), 19606–19615 (2013).
11. M. W. Knight, N. S. King, L. Liu, H. O. Everitt, P. Nordlander, and N. J. Halas, "Aluminum for plasmonics," ACS Nano **8**(1), 834–840 (2014).
12. H. Ehrenreich, H. R. Philipp, and B. Segall, "Optical properties of aluminum," Phys. Rev. **132**(5), 1918–1928 (1963).
13. H. Raether, *Surface Plasmons on Smooth and Rough Surfaces and on Gratings*, Springer Tracts in Modern Physics (Springer-Verlag, 1988), Vol. 111.

#294948 https://doi.org/10.1364/OME.7.002880
Journal © 2017 Received 1 May 2017; revised 30 Jun 2017; accepted 3 Jul 2017; published 12 Jul 2017

Optical Materials EXPRESS

14. G. H. Chan, J. Zhao, G. C. Schatz, and R. P. Van Duyne, "Localized surface plasmon resonance spectroscopy of triangular aluminum nanoparticles," J. Phys. Chem. C **112**(36), 13958–13963 (2008).
15. K. Appusamy, S. Blair, A. Nahata, and S. Guruswamy, "Low-loss magnesium films for plasmonics," Mater. Sci. Eng. B **181**, 77–85 (2014).
16. F. Sterl, N. Strohfeldt, R. Walter, R. Griessen, A. Tittl, and H. Giessen, "Magnesium as novel material for active plasmonics in the visible wavelength range," Nano Lett. **15**(12), 7949–7955 (2015).
17. K. Appusamy, X. Jiao, S. Blair, A. Nahata, and S. Guruswamy, "Mg thin films with Al seed layers for UV plasmonics," J. Phys. D Appl. Phys. **48**(18), 184009 (2015).
18. H.-H. Jeong, A. G. Mark, and P. Fischer, "Magnesium plasmonics for UV applications and chiral sensing," Chem. Commun. (Camb.) **52**(82), 12179–12182 (2016).
19. M. Santamaria, F. Di Quarto, S. Zanna, and P. Marcus, "Initial surface film on magnesium metal: A characterization by X-ray photoelectron spectroscopy (XPS) and photocurrent spectroscopy (PCS)," Electrochim. Acta **53**(3), 1314–1324 (2007).
20. A. V. Krasavin, K. F. MacDonald, N. I. Zheludev, and A. V. Zayats, "High-contrast modulation of light with light by control of surface plasmon polariton wave coupling," Appl. Phys. Lett. **85**(16), 3369–3371 (2004).
21. J. M. McMahon, G. C. Schatz, and S. K. Gray, "Plasmonics in the ultraviolet with the poor metals Al, Ga, In, Sn, Tl, Pb, and Bi," Phys. Chem. Chem. Phys. **15**(15), 5415–5423 (2013).
22. Y. Yang, J. M. Callahan, T.-H. Kim, A. S. Brown, and H. O. Everitt, "Ultraviolet nanoplasmonics: a demonstration of surface-enhanced Raman spectroscopy, fluorescence, and photodegradation using gallium nanoparticles," Nano Lett. **13**(6), 2837–2841 (2013).
23. J. Wang, S. Liu, S. Guruswamy, and A. Nahata, "Injection molding of free-standing, three-dimensional, all-metal terahertz metamaterials," Adv. Opt. Mater. **2**(7), 663–669 (2014).
24. Y. Yang, N. Akozbek, T.-H. Kim, J. M. Sanz, F. Moreno, M. Losurdo, A. S. Brown, and H. O. Everitt, "Ultraviolet–visible plasmonic properties of gallium nanoparticles investigated by variable-angle spectroscopic and Mueller matrix ellipsometry," ACS Photonics **1**(7), 582–589 (2014).
25. T. Castro, R. Reifenberger, E. Choi, and R. P. Andres, "Size-dependent melting temperature of individual nanometer-sized metallic clusters," Phys. Rev. B Condens. Matter **42**(13), 8548–8556 (1990).
26. W. R. Tyson and W. A. Miller, "Surface free energies of solid metals: Estimation from liquid surface tension measurements," Surf. Sci. **62**(1), 267–276 (1977).
27. P. Guex and P. Feschotte, "Les systèmes binaires platine-aluminium, platinegallium et platine-indium," J. Less Common Met. **46**(1), 101–116 (1976).
28. T. B. Massalski, H. Okamoto, and A. S. M. International, *Binary Alloy Phase Diagrams* (ASM International, 1990).
29. M. Li, C. Li, F. Wang, and W. Zhang, "Thermodynamic assessment of the Ga–Pt system," Intermetallics **14**(7), 826–831 (2006).
30. M. M. Yazdanpanah, V. V. Dobrokhotov, A. Safir, S. Pabba, D. Rojas, and R. W. Cohn, "Room temperature growth of single intermetallic nanostructures on nanoprobes," The 11th Annual NSTI Nanotech, Boston, MA, **1**, 896–899 (2008).
31. R. W. Cohn, "Freestanding metallic and polymeric nanostructures: Directed self-assembly," in *Dekker Encyclopedia of Nanoscience and Nanotechnology, Third Edition* (CRC Press, 2014), pp. 1450–1474.
32. M. W. Knight, T. Coenen, Y. Yang, B. J. M. Brenny, M. Losurdo, A. S. Brown, H. O. Everitt, and A. Polman, "Gallium plasmonics: deep subwavelength spectroscopic imaging of single and interacting gallium nanoparticles," ACS Nano **9**(2), 2049–2060 (2015).
33. T. Matsui, A. Agrawal, A. Nahata, and Z. V. Vardeny, "Transmission resonances through aperiodic arrays of subwavelength apertures," Nature **446**(7135), 517–521 (2007).
34. T. W. Ebbesen, H. J. Lezec, H. F. Ghaemi, T. Thio, and P. A. Wolff, "Extraordinary optical transmission through sub-wavelength hole arrays," Nature **391**(6668), 667–669 (1998).

1. Introduction

The field of plasmonics has grown tremendously in recent years, with demonstrations of device technologies relevant to a broad range of research topics that include physics, chemistry, materials science, engineering and bioscience [1–4]. The success of this approach relies fundamentally on using metals with dielectric properties that allow for strong enhancement of the electromagnetic field, while also minimizing propagation losses. The relevance of plasmonics for the UV spectral range arises from the fact that a wide variety of excitations may be found within this region that can be used to understand the structural, conformational and kinetic properties of materials. In the case of biomolecules, although they absorb in the UV, they often exhibit relatively low quantum efficiencies and molar extinction coefficients [5,6]. Achieving significant enhancement of the electromagnetic field through the use of plasmonic structures [7] may allow for label-free studies of a wide variety of molecules. More generally, UV plasmonics can be applied to topics including photocatalysis

Optical Materials EXPRESS

[8], surface-enhanced resonance Raman scattering [9], and photodegradation acceleration [10].

In the visible and near-infrared spectral regions, the metals most commonly used are Ag and Au. As one moves to higher frequencies, corresponding to the ultraviolet (UV) spectral range, these metals are no longer suitable for plasmonics applications because of interband transitions. Aluminum, on the other hand, has been widely studies for UV plasmonics application [11], since the onset of interband transitions do not occur until ~1.4 eV [12]. This dampens the visible response relative to Au and Ag, but does not strongly affect the response from the blue to the deep UV (< 200 nm). There are, however, issues with surface roughness of thin films, which can lead to surface plasmon-polariton (SPP) damping [13]. In addition, Al forms a thin native oxide, which can affect the resonance of plasmonic devices [14]. Recently, Mg has been shown to be an attractive metal for UV plasmonics applications [15–18]. However, the formation of $Mg(OH)_2$ destroys the film in humid environments [19]. Therefore, it is important to investigate and develop other materials for this important frequency range.

Gallium is another attractive plasmonic material that has an added advantage of allowing for changes in its dielectric properties via thermally-driven phase transitions at close to room temperature [20–22]. In bulk form, the metal can be easily melted and reshaped to yield the desired geometry [23]. However, Ga does not easily wet most common substrates, including Si and a variety of glasses, making vacuum deposition of thin, continuous Ga films extremely challenging. Moreover, Ga is detrimental to many metals and Al, in particular, as it causes severe metal embrittlement. Thus, vacuum deposition of Ga usually requires a dedicated chamber, so as to not contaminate other commonly deposited metals. Even when this is done, the deposition of Ga or one of its alloys results in a substrate surface covered with isolated metal nanoparticles [22,24]. While such structures have proven useful for the study of localized surface plasmon resonances and enhanced Raman scattering in the UV [22,24], they are not useful for a broad range of applications that rely on propagating SPPs.

In this submission, we demonstrate a simple method to produce thin, continuous films of gallium-platinum alloys. Importantly, these films retain much of the attractive plasmonic properties of pure gallium in the UV. The films are produced by first vacuum depositing a Pt wetting layer on a quartz substrate and then manually spreading a thin Ga layer on top. When the excess Ga is removed, a thin (typically less than 100 nm thick) alloy film in which the Ga/Pt composition is graded remains. We used energy dispersive spectroscopy (EDS) to characterize the alloy composition and ellipsometry to measure the UV refractive index properties in the range 250 nm – 500 nm. We also fabricated a periodic array of subwavelength apertures to demonstrate the plasmonic properties of the medium. It is also interesting to note that the different Ga-Pt alloys all have melting temperatures that are substantially higher than that of pure Ga. This alleviates a significant issue that would exist for pure Ga thin films: processing steps that require that the temperature go above 30° C would cause Ga to melt, making the retention of metal nanostructuring difficult.

2. Theory

We examined the wettability of Ga on Pt substrates through first-principles surface and interface energies (γ) calculations using density functional theory. Using the VASP package [25], we adopted the projector augmented wave method in conjunction with a local density approximation for electron exchange and correlation. The kinetic energy cutoff for the plane wave basis was set to 400 eV. We used orthorhombic symmetry to set the crystal structure of Ga and cubic symmetry for Pt. To calculate the surface energy, the Ga and Pt surfaces were modeled using a slab geometry along the (011) direction with a thickness of ~1 nm. To calculate the interface energy, a Ga 2x1x6 (2x1x8) supercell was put on a Pt 2x2x7 (2x2x9) supercell to minimize the lattice mismatch. For the Ga-Pt interfaces, several different interface configurations were selected to determine the lowest energy. We also ensured that

Optical Materials EXPRESS

the k-point mesh was sufficient for the Brillouin zone integration. All of the structures were fully relaxed until the atomic forces were smaller than 0.01 eV/Å.

We obtained surface energies for Ga and Pt of 0.69 and 2.37 J/m^2, respectively, which are in good agreement with previous experimental and theoretical results [25,26]. In addition, we found that the Ga-Pt interfacial energy was −1.22 J/m^2. Based on these results, thermodynamically, Ga should wet Pt surfaces at low temperature, because the wetting condition of γ(substrate) > γ(film) + γ (interface) is satisfied. We also examined other metals as potential wetting layers. Au was the most similar to Pt. However, Ga was found to exhibit better wetting on Pt than on Au, because Pt exhibits a much higher surface energy than Au. Furthermore, the Ga-Pt interface energy is lower than the Ga-Au interface energy. The lower Ga-Pt interface energy also indicates a strong tendency for mixing between Ga and Pt during growth of Ga on Pt.

3. Experimental details

The basic process for producing thin, continuous Ga alloy thin films is shown schematically in Fig. 1(a). We first vacuum deposited a 3 nm layer of Cr onto a quartz substrate, followed by a 10 nm Pt wetting layer using DC sputtering. We then manually spread a thin layer of Ga onto the Pt film using the edge of a glass slide. The resulting Ga film was not uniform, but there were regions where the layer had an average thickness of approximately 1μm. In order to expose the alloy film in those regions, we thinned a 10 μm x 10 μm square region by milling away the excess Ga with a focused ion beam (FIB). To accomplish this, we initially used an ion beam current of 230 pA. This process typically took less than two minutes. Ga was removed rapidly until the ion beam reached the interface between the bulk Ga and the Ga-Pt alloy, at which point the removal rate decreased dramatically. Therefore, we could halt the milling process when the well depth stopped changing by simply monitoring the SEM image of the milled region. This typically resulted in a film thickness of ~100 nm. We then reduced the FIB beam current to 40 pA to further smooth the surface at the bottom of the square well. An image of the resulting structure is shown in Fig. 1(b). It should be noted that after milling, the geometry of the well sidewalls did not change over time, indicating that the structure was stabilized.

Before fabricating plasmonic structures in the alloy thin films, we performed ellipsometry measurements on both the top and bottom surfaces of the alloy film. The measurements were performed using a Woollam Variable Angle Spectroscopic Ellipsometer (VASE). We performed topside and backside measurements of the sample. Measurements of the amplitude ψ and phase change Δ were taken in the wavelength range of 260nm-800nm with incident angles of 70° and 75°. The refractive index n and extinction coefficient k were obtained by fitting the experimental data. The dielectric constants ε_r (real part) and ε_i (imaginary part) were calculated from n and k.

Finally we fabricated 10 μm x 10 μm periodic arrays of subwavelength apertures via FIB milling within each square well. Three different sets of arrays were fabricated with periodicities of 300 nm (100 nm diameter apertures), 600 nm (300 nm diameter apertures) and 650 nm (300 nm diameter apertures). An image of a portion of the 300 nm periodicity sample is shown in Fig. 1(c). Some regions of the image appear darker than other regions. We do not know the origin of this difference, but speculate that it is associated with the alloy composition. We used two separate optical systems with different light sources and detectors to measure the transmission properties in the spectral ranges extending from 250 nm – 400 nm and from 450 nm – 800 nm. Thus, direct comparison of the transmission magnitudes is not possible.

Optical Materials EXPRESS

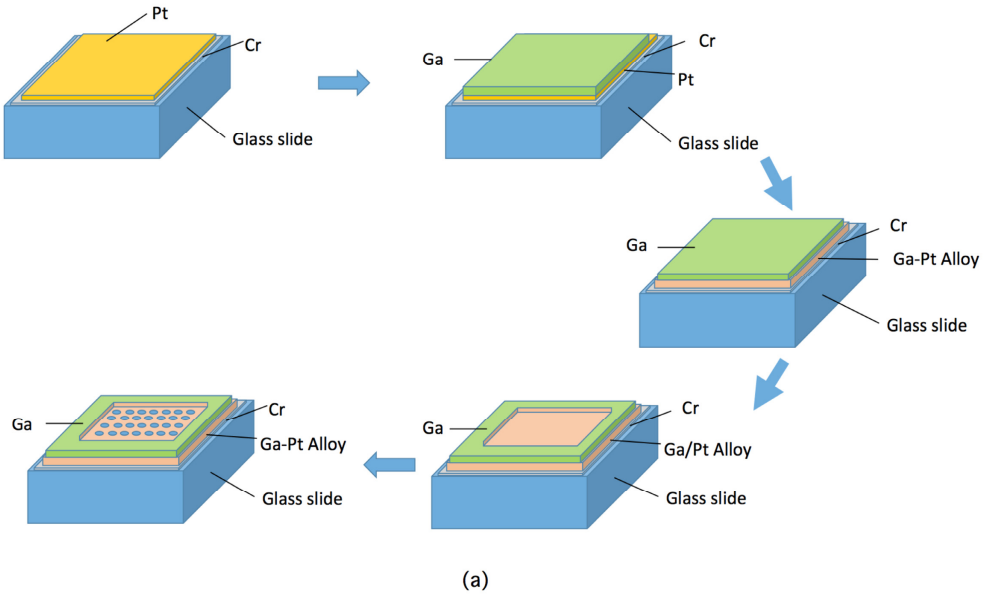

(a)

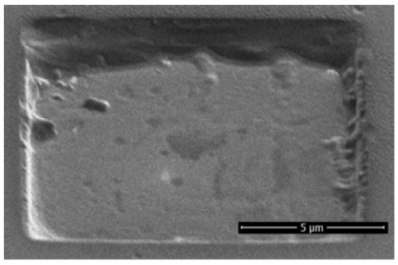

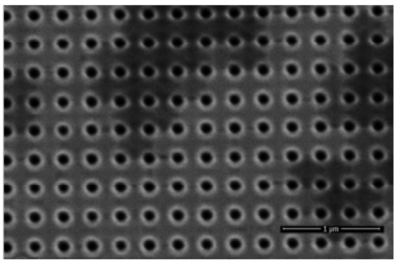

(b) (c)

Fig. 1. (a) Schematic diagram of the process used to create continuous thin films of Ga-Pt and subwavelength aperture arrays. A 3 nm Cr adhesion layer is first deposited onto a quartz slide, followed by a 10 nm layer of Pt (or Au) as a wetting layer. A Ga film is then manually spread on top of the wetting metal using the edge of a quartz slide, enabling the formation of a Ga-Pt thin film. The overall film thickness is approximately 1 µm. The excess Ga is then removed using FIB milling within a square well, exposing the ~100 nm thick alloy layer. To create plasmonic structures, the FIB is used once again to pattern the alloy thin film. (b) Scanning electron micrograph of a 10 µm x 10 µm exposed Ga-Pt film at the bottom of a well created by milling away the excess Ga. (c) and (b) Scanning electron micrograph of a subwavelength aperture array fabricated in the exposed Ga-Pt thin film. The apertures are circular with a diameter of 100 nm and periodicity of 300 nm.

4. Results and discussion

We begin by discussing the composition of the alloy film. In general, the solubility of Pt in Ga tends to be small. Nevertheless, when Pt comes into contact with Ga in the solid phase, a number of different intermetallic compounds form at room temperature: Ga_6Pt, Ga_7Pt_3, Ga_2Pt, Ga_3Pt_2, GaPt, Ga_3Pt_5, $GaPt_2$ and $GaPt_3$ [27–29]. It is important to note that the Ga film does not need to be in the liquid state for this alloying process to take place. The low interfacial energy of the Ga-Pt interface allows the formation of a continuous Ga_6Pt intermetallic compound in equilibrium with Ga that has an orthorhombic crystal structure up to the peritectic temperature of 291°C [27–29]. In this structure, the 10 nm thick Pt layer in contact

Optical Materials EXPRESS

with thick Ga is expected to form Ga_6Pt. Indeed, Ga in contact with Pt has been observed to readily form Ga_6Pt nanocrystals at room temperature [30,31]. We used energy dispersive x-ray spectroscopy (EDS) to measure the relative concentration of Ga and Pt as a function of the alloy film depth, shown in Fig. 2, demonstrating the change in the Ga/Pt ratio with film depth. It should be noted that the observed composition is dependent upon the sample geometry and beam spread within the transmission electron microscope (TEM).

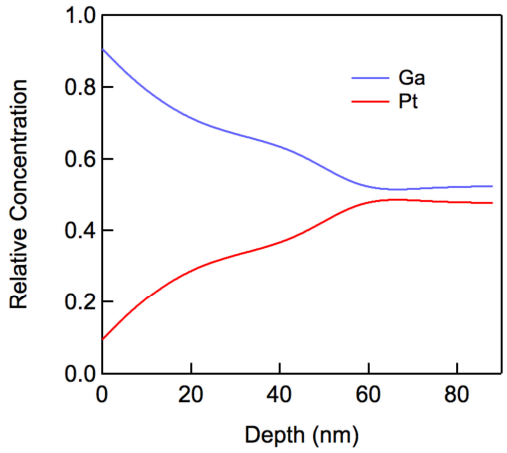

Fig. 2. EDS analysis for the relative concentration of Ga and Pt in the alloy film. The substrate is at the right end of the graph.

We used ellipsometry to measure the dielectric properties of the Ga-Pt thin film. In these measurements, the reflection coefficient is given by

$$\rho = \frac{r_p}{r_s} = \tan\psi \exp[i\Delta] \tag{1}$$

where r_p and r_s are the reflection coefficients for s- and p-polarized light, tan ψ corresponds to $|r_p / r_s|$ and Δ is the phase difference between the two polarizations. From the Fresnel equation and Snell-Descartes Law, the refractive index of substrate can be calculated from the relationship

$$n = n + ik = \sin\phi_o \left[1 + \left(\frac{1-\rho}{1+\rho} \right)^2 \tan^2 \phi_o \right]^{1/2}, \tag{2}$$

where φ_0 is the incident angle and $\varepsilon = (n + ik)^2$. From the measurements of ψ and Δ, and model for the sample structure, we can fit the measured data to extract n and k. In the measurements, data was collected at incident angles of 70° and 75°. We used a two-layer model. As a starting point, we assumed a 1 mm thick SiO_2 substrate, with light illumination from the substrate side, and a 1 μm thick aluminum layer. We did this to model the Ga-Pt thin layer, since no standard model for our alloy film exists in the Woollam library. Refractive indices of n and k were then obtained by normal fitting. The optical constants of solid Ga were measured using reflection from the Ga film, and the model only involved one layer of Al to model Ga. We found that our measurements of dielectric constants are similar to others' work, which implies that our model and data fits are reasonable [32].

In Fig. 3, we show the real, ε_r, and imaginary, ε_i, components of the dielectric constant measured from the top and bottom surfaces of the film deposited on the quartz slide, along with published data for pure Ga in both solid and liquid forms. As shown in the figure, the top

Optical Materials EXPRESS

(alloy-air) surface of the film exhibits dielectric properties essentially match those of solid Ga over the entire measured spectral range from 250 nm – 800 nm. This is not surprising, since the top layer is pure Ga that will be removed prior to nanopatterning. The dielectric properties of the bottom (alloy-quartz) surface are also reasonably similar to those of pure Ga, but only over the 250 nm – 550 nm wavelength range. Although we expect only alloys of Ga and Pt at the interface, the results demonstrate that Ga-Pt alloys largely retain the advantageous optical properties of Ga, despite the fact that Pt is known to be a poor plasmonic metal in the UV. In fact, the difference in dielectric constants of solid Ga and the Ga-Pt alloy is less than 10% in the spectra range of 260 nm – 450 nm.

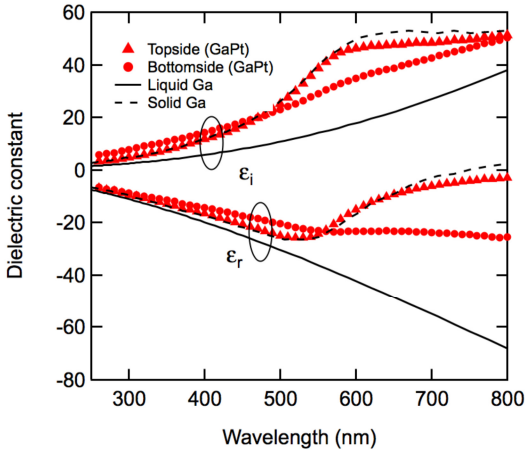

Fig. 3. Dielectric properties of the Ga-Pt thin film measured using ellipsometry from both the top (alloy-air) surface and bottom (alloy-quartz) surface. Dielectric properties for solid and liquid Ga are also shown for comparison [32].

In Fig. 4, we show the transmission spectra for the three separate aperture arrays, along with measurements performed after six months for the array that had 650 nm periodicity. For a periodic array, we have previously shown that the dip on the high frequency side of the resonance [33] is the fundamental parameter of the resonance. This wavelength is given by [34]

$$\lambda_{dip} = \frac{Pn_{SPP}}{\sqrt{i^2 + j^2}}, \tag{3}$$

where P is the aperture periodicity, i and j are integers and n_{SPP} is the SPP effective refractive index given by

$$n_{SPP} = \sqrt{\frac{\varepsilon_m \varepsilon_d}{\varepsilon_m + \varepsilon_d}}. \tag{4}$$

Here, ε_m and ε_d are complex dielectric constants of the metal and dielectric media. For the array with P = 300 nm, the first order resonance (i = ± 1 and j = 0 or i = 0 and j = ± 1) yields a dip at 316 nm for the alloy-air interface and the (i = ± 1 and j = ± 1) resonance yields a dip at 330 nm for the alloy-quartz interface. These two resonances cannot be distinguished from the measured transmission, but agree with the measured dip at 325 nm. We observe similar agreement for the other two arrays measured in the visible spectral range. As noted above, the transmission properties of the 300 nm periodicity sample were measured using a different optical system from the other two samples. Nevertheless, the spectrum in Fig. 4(a) exhibits a sharper resonance than those in Fig. 4(b). This is not surprising, given that the metal exhibits dielectric properties that are closer to that of Ga only in the UV. Finally, we assessed the

Optical Materials EXPRESS

environmental stability of the Ga-Pt alloys through measurement of the plasmonic properties over time. We stored the 650 nm period sample in a container with air and desiccant for 6 months and repeated the transmission measurement. While there is some difference in the spectral properties, the results are qualitatively similar to the fresh sample. These results indicate that Ga-Pt film is stable in dry air.

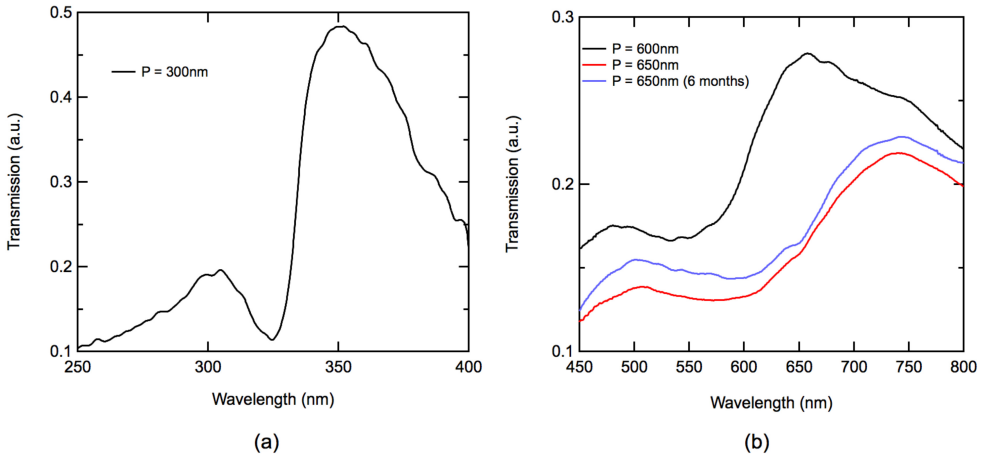

Fig. 4. Optical transmission spectra measured for three separate 10μm x 10μm area Ga-Pt aperture array structures with different aperture diameters and periodicities. (a) UV transmission measured for an aperture array with aperture diameters of 100 nm and a periodicity of 300nm. (b) Visible transmission measured for the samples with periodicity of 600 nm and 650 nm and aperture diameters of 300nm in both cases. The transmission spectrum measured for the 650 nm periodicity sample after 6 months is also shown.

5. Conclusion

In conclusion, we developed a method to create Ga alloy based pinhole-free thin films that largely retain the favorable dielectric properties of pure Ga, especially in the UV spectral region. We accomplished this by first depositing a thin Pt seed layer and then spreading a thicker Ga layer on top. The resulting Ga-Pt alloy formed with a thickness of ~100 nm, starting from the substrate interface; the remaining upper layer of pure Ga and could be removed by FIB milling and polishing. We demonstrated the utility of this alloy material for plasmonics, by fabricating a variety of periodic subwavelength aperture arrays and measuring the optical transmission properties. The spectral resonances were consistent with expectations. Interestingly, the resonances were sharper in the UV than in the visible, which was consistent with the fact that the dielectric properties of the alloy diverged from those of solid Ga in the visible. These films appear to be environmentally stable over reasonably long periods of time in ambient conditions. Thus, these materials are promising for plasmonics applications in the UV.

Funding

National Science Foundation (NSF) (1121252).

Acknowledgment

This work made use of University of Utah USTAR shared facilities supported, in part, by the MRSEC Program of NSF under Award No. DMR-1121252. We thank Brian R. Van Devener, Paulo Perez and Randy C. Polson for technical assistance with the FIB and ellipsometry facilities.